Apoptosis (2025) 30:55–68
https://doi.org/10.1007/s10495-024-02019-3

# Anti-PD-L1 blockade facilitates antitumor effects of radiofrequency ablation by improving tumor immune microenvironment in hepatocellular carcinoma

**Jiahua Liang[1,2] · Mingjian Ma[1] · Wei Feng[1] · Qiongcong Xu[1] · Dong Chen[1] · Jiaming Lai[1] · Jiancong Chen[1]**

Accepted: 13 September 2024 / Published online: 26 September 2024


**Abstract**

Hepatocellular carcinoma (HCC) is a complex disease with advanced presentation that significantly affects survival rates. Therefore, novel therapeutic strategies are needed. In this study, we investigate the tumor microenvironment (TME) in HCC by analyzing 13 HCC samples at single cell level. We identified key cell populations, including CD8 + T cells, Tregs, M1/M2 macrophages, and CD4 + memory T cells, and explored their roles and interactions. Our research revealed an early enrichment of CD8 + T cells, which could potentially lead to their exhaustion and facilitate tumor progression. We also investigated the impact of percutaneous radiofrequency ablation (RFA) on the immune microenvironment. Using a dual tumor mouse model, we demonstrated that RFA induces necrosis, enhancing antigen presentation and altering immune responses. Our results indicate that RFA increases PD-L1 expression in residual liver tissue, suggesting potential immune escape mechanisms. Furthermore, the combination of RFA and anti-PD-L1 therapy in the mouse model resulted in significant improvements in immune modulation. This included increased CD8 + T cell efficacy and decreased Treg infiltration. This combination shows promise as an approach to counteract HCC progression by altering the immune landscape. This study highlights the critical interaction within the TME of HCC and suggests the possibility of improving patient outcomes by targeting immune evasion mechanisms through combined therapeutic strategies.

**Keywords** Hepatocellular carcinoma · Radiofrequency ablation · Single cell analysis · Tumor immune microenvironment · Anti-PD-L1 blockade

## Introduction

Hepatocellular carcinoma (HCC) is a primary liver cancer with high mortality rates [1]. Patients with early-stage HCC who are ineligible for surgery often opt for ablation therapies such as radiofrequency ablation (RFA), which is most effective for tumors less than 3 cm in size. RFA induces immunogenic cell death, potentially stimulating local anti-tumor immunity [2, 3]. However, for larger tumors or tumors close to blood vessels, RFA may not achieve complete ablation, leading to recurrence or metastasis due to an inadequate immune response.

Current knowledge indicates that percutaneous ablation techniques, such as RFA and microwave ablation (MWA), not only induce direct tumor necrosis but also modulate the immune system. These procedures trigger an inflammatory response by releasing tumor antigens and damage-associated molecular patterns(DAMPs), which subsequently stimulate both innate and adaptive immune responses. Dumolard et al. reported increased immune cell infiltration within the tumor microenvironment after ablation [4]. Mizukoshi et al. found that RFA increases tumor-specific T cells, particularly CD8 + T cells [5]. Additionally, combining ablation with

Jiahua Liang, Mingjian Ma and Wei Feng contributed equally to this work.

✉ Jiaming Lai
laijm@mail.sysu.edu.cn

✉ Jiancong Chen
chenjc25@mail.sysu.edu.cn

[1] Department of Pancreato-Biliary Surgery, The First Affiliated Hospital, Sun Yat-sen University, Guangzhou 510080, China

[2] Department of Medicine II, Medical Faculty Mannheim, Universitätsmedizin Mannheim, Heidelberg University, Mannheim, Germany

immunotherapy can enhance anti-tumor immunity and prevent recurrence, as reviewed by Li et al. [6]

The abscopal phenomenon refers to a rare systemic response where localized radiation therapy (RT) on a primary tumor leads to regression of distant metastases. This effect is mediated by the immune system. RT induces immunogenic cell death, releasing tumor antigens and cytokines that activate dendritic cells and T-cells, thus generating a systemic anti-tumor response [7]. In clinical settings, the abscopal effect has been documented in various cancers, including melanoma and non-small cell lung cancer (NSCLC). These responses usually occur within months of RT, indicating a synergistic effect between RT and immunotherapy [8].

Recent studies emphasize the importance of the tumor microenvironment (TME) in HCC, particularly the role of $CD8^+$T cells, regulatory T cells (Tregs), and M1/M2 macrophage polarization in disease progression and treatment response. After radiofrequency ablation, the tumor microenvironment experiences significant changes. The activity of $CD8^+$T cell may be affected, which can impact their ability to response cytotoxically. Additionally, regulatory T cell within the TME have the potential to suppress anti-tumor immunity. Furthermore, changes in macrophage polarization toward either a pro-inflammatory M1 phenotype or an immunosuppressive M2 phenotype may influence tumor recurrence and patient outcomes. M1 macrophages promote inflammation that targets tumor cells, while M2 macrophages often support tumor growth and contribute to immune evasion [9]. After RFA, an increase in immunosuppressive cells like polymorphonuclear myeloid-derived suppressor cells (PMN-MDSCs) has been observed, which diminishes $CD8^+$T cell activity. Modifying the TME could potentially improve HCC management post-RFA [10]. Further exploration is necessary to enhance therapeutic strategies and improve prognosis, given the intricate interplay between these components and their collective impact on HCC pathogenesis and treatment response, especially following RFA [11].

The microenvironment that follows radiofrequency ablation is immunosuppressive and involves complex interactions between immune cells, which are not yet fully understood. Recent evidence has shown a significant increase of PD-L1 expression in this context, highlighting its potential as a therapeutic target [12–14]. Recent studies indicate that PD-L1 is expressed not only by tumor cells but also by various immune cells, including dendritic cells (DCs) and macrophages, in both human and mouse models. In human cancers, particularly lung adenocarcinoma, PD-L1 expression on macrophages has been shown to contribute significantly to immune suppression and the tumor microenvironment. Similarly, research in murine models has demonstrated that PD-L1 on DCs plays a crucial role in regulating antitumor T cell responses through interactions with CD8 + T cells. This regulation affects T cell priming and expansion, highlighting the complex role of PD-L1 beyond simply reversing T cell exhaustion [15].Our research aims to explore the details of the tumor microenvironment after RFA to improve the clinical effectiveness of combining RFA with anti-PD-L1 therapy. We investigate the complex communication between diverse immune cells and evaluate the effects of targeted therapies. Our goal is to uncover the mechanisms that drive immune cell dynamics and discover new approaches to enhance anti-tumor responses, ultimately improving patient outcomes in the treatment of hepatocellular carcinoma.

## Methods

### Single-cell data sources and quality enhancement

The datasets GSE112271, GSE210679, and GSE242889, comprising single-cell RNA sequencing data from 13 hepatocellular carcinoma specimens, were meticulously acquired using the 10X Genomics platform (Supplementary Table). To analyze the scRNA-seq data, a systematic series of analytical steps was followed. The initial step involved preprocessing the scRNA-seq data with the "Seurat" software package. Various methods were then employed, including the PercentageFeatureSet function, to assess the proportion of mitochondrial gene expression. Additionally, correlation analyses were performed to explore the relationships among sequencing depth, mitochondrial gene frequencies, and total intracellular gene counts.

To ensure the integrity of the analysis, a stringent gene filtration strategy was implemented, requiring that genes be expressed in at least five cells. Moreover, strict criteria were applied to select cells with a gene expression profile of more than 300 but fewer than 5000 genes, less than 10% mitochondrial gene content, and a minimum of 1000 unique molecular identifiers (UMIs) per cell. Following this careful data curation, the scRNA-seq datasets were normalized using the LogNormalize method to enhance the accuracy of subsequent analyses and interpretations.

### In-depth single-cell transcriptome analysis

Fifteen principal components were identified through principal component analysis, utilizing the 2,000 most variably expressed genes to minimize batch effects from different dataset origins. The dataset was further refined using Harmony, t-SNE, and UMAP methodologies to enable unsupervised clustering and the identification of cellular

subpopulations within a two-dimensional framework. Differential gene expression among clusters was analyzed with the "FindAllMarkers" function, applying a significance threshold of an absolute log2 fold change greater than 1 and an adjusted P-value below 0.05. The resolution parameter was set at 1.0 to achieve precise cluster delineation. The resulting clusters were classified into known cellular phenotypes using CellMarker 2.0, based on characteristic marker genes. Additionally, the CellChat R package was employed to elucidate the complex network of cell-to-cell communication, offering a comprehensive understanding of intercellular signaling networks.

## Cell lines

The Hepa1-6 mouse hepatoma cell line was obtained from the American Type Culture Collection (ATCC) cell bank. The culture medium was supplemented with 10% fetal bovine serum and 1% penicillin-streptomycin (Gibco).

## Cell transfection

A lentiviral vector containing the luciferase gene was engineered and synthesized by Shanghai Hanheng Biotechnology Co., Ltd. Lentiviral packaging was performed using 293T cells, and the collected supernatant was used to transfect Hepa1-6 cells. Resistant clones were selected 24 h post-transfection using puromycin [16].

## Establishment of liver tumor in situ in C57BL/6L mice

The mouse hepatoma cell line Hepa1-6-Luc cells were suspended in PBS at a density of 1 × 10^6 cells /ml. C57BL/6J mice aged 4–5 weeks were anesthetized and their abdomen was disinfected with iodophos. A small incision of approximately 0.8 cm was made in the abdominal skin, and the left and middle lobes of the liver were exposed. A 25ul cell suspension was injected slowly using a 1 ml syringe to form tumors in the left and middle lobes of the liver. After injection, the injection site was pressed with a cotton ball and the needle was removed. The abdomen was then closed layer by layer after confirming no bleeding. Tumor growth was observed in situ by intraperitoneal injection of substrate fluorescein every 3 days.

## Radiofrequency ablation of liver tumors in situ

The mice were anesthetized and positioned to expose the abdomen through the original incision. The upper frequency limit was set to 7 W, and the temperature was maintained at 70 °C. After the instrument setup, a unipolar radio frequency probe (17G) was inserted into the center of the tumor along its longitudinal axis, and the power was activated. The left lobar liver tumor was fully ablated for 10–20 s once the temperature at the ablation needle tip, monitored automatically, reached 60 °C. The maximum temperature was controlled between 70 and 80 °C. Half of the mice underwent complete radiofrequency ablation of the left lobar tumor, while the other half served as a control group and underwent only abdominal incision and closure. Mice were euthanized by cervical dislocation on days 3 and 6 post-radiofrequency ablation, and liver tissue was collected from all mice.

## RFA and anti-PD-L1 combined therapy in tumor-bearing mice

Mice were injected with liver cancer cells to induce tumors both in the liver (single tumor in the left lobe) and subcutaneously. To establish the subcutaneous tumor model, 0.2 ml of a prepared liver cancer cell suspension (1 × 10^6 cells/ml) was drawn into a 1 ml syringe and injected into the subcutaneous tissue of the mice. Once the intrahepatic tumor reached a diameter of approximately 0.8–1 cm (achieved in about 7–8 days, as confirmed by in vivo fluorescence imaging), the tumor-bearing mice were randomly assigned to one of four groups: RFA + Anti-PD-L1, RFA only, Anti-PD-L1 only, and untreated. Starting the day after RFA treatment, mice received intraperitoneal injections of 200 µg (25 µl) of anti-PD-L1 monoclonal antibody every three days for a total of four injections. Tumor growth and survival time were subsequently monitored and recorded.

## Collection of tumor infiltrating cells

After completely removing the central liver tumor, we diluted specified amounts of collagenase I and IV, hyaluronidase, and DNase were diluted in DMEM medium and used them for enzymatic digestion of tumor tissue. The tissue was then incubated at 37 °C for 2 h. Next, we transfected the tissue to a sterile glass petri dish and mechanically dissociated it to create a homogenate. The cell suspension was then filtered through a 40 µm mesh to remove particulate debris and cellular aggregates. Then the resulting cell suspension was washed and re-suspended to obtain a homogeneous single-cell suspension suitable for downstream applications. The characterization and quantification of immune cell subsets within the suspension were characterized and quantified through immunophenotyping using flow cytometry and specific staining protocols.

### Flow cytometry

The study utilized a Beckman-Coulter flow cytometer equipped with blue (488 nm), red (640 nm), and violet (405 nm) lasers to detect various fluorochromes. Flow cytometry controls included unstained cells to establish background fluorescence and isotype controls (IgG2b - FITC, IgG2b - PE-Cy5, IgG2α - PE-Cy7, IgM - PE, IgG2α - PE, IgG2α - PE-Cy7 from eBioscience) to determine non-specific binding. FlowJo software was used for collecting and analyzing the FACS data. The specific antibodies and fluorochromes used in the flow cytometry panels were: Anti-mouse CD3 - FITC (Biolegend), Anti-mouse PD-L1 - PE (Biolegend), Anti-mouse CD4 - ECD (eBioscience), Anti-mouse FoxP3 - FITC (eBioscience), Anti-mouse CD8 - APC (eBioscience), Anti-mouse CD45 - AF-700 (eBioscience), Anti-mouse TNF-α - PE (Biolegend), Anti-mouse IFN-γ - FITC (Biolegend), Anti-mouse Gr1 - FITC (eBioscience), Anti-mouse CD11c - PE (Biolegend), Anti-mouse Ly6G - PE-594 (Biolegend), Anti-mouse PD-L1 - PC7 (Biolegend), Anti-mouse F4/80 - APC (Biolegend), Anti-mouse CD11b - AF-700 (Biolegend), Anti-mouse Ly6C - BV-421 (Biolegend), Anti-mouse CD45 - BV-570 (Biolegend) [17–19].

The prepared cell suspension was adjusted to a concentration of $5.0 \times 10\text{^}6$ cells/ml. Then, 100 µl of the cell suspension was added to each EP tube, followed by the corresponding fluorescently labeled detection antibody, mixed according to the instructions. After incubating at 4 °C for 30 min and washing away the unbound antibody with PBS, 300 µl of PBS was added, mixed, and transferred to the flow tube for machine detection.

### IFN-γ and TNF-α staining

Phorbol 12-myristate 13-acetate (PMA) and ionomycin were prepared at working concentrations of 50 ng/ml and 1 µg/ml, respectively. The cells were then harvested and re-suspended in DMEM medium supplemented with 1% Fetal Calf Serum (FCS), 50 ng/ml PMA, and 1 µg/ml ionomycin. The cell suspension was then allocated into a 24-well plate and incubated at 37 °C for 1 h. After incubation, the termination solution was added, and the culture was continued for an additional 3–4 h. The cells were resuspended every 30 min. Following stimulation, the cells were collected and washed once with Phosphate-Buffered Saline (PBS) containing 1% FCS, followed by a subsequent wash with PBS alone. The cells were initialy labeled with a specific antibody and washed with PBS before decarding the supernatant. Subsequently, 200 µl of fixation solution A was added, and the cells were incubated at 4 °C in the dark for 15 min. After fixation, the cells were washed with 1X permeabilization solution B. The interferon gamma (INF-γ) antibody, pre-diluted in permeabilization solution B, was added to the cells and incubated at 4 °C, protected from light, for 25 min. Following incubation, the cells were centrifuged, washed with PBS, and re-suspended for analysis by flow cytometry. Similarly, for the analysis of tumor necrosis factor alpha (TNF-α), the TNF-α antibody, pre-diluted in permeabilization solution B, was added to the cells and incubated at 4 °C, protected from light, for 25 min. After incubation, the cells were centrifuged, washed with PBS, and re-suspended for analysis by flow cytometry.

### Statistical analysis

Statistical analyses of the experimental outcomes were conducted using SPSS software version 23.0. Data were presented as mean ± standard deviation. Normality tests were performed to ascertain whether the sample data conformed to a normal distribution. For comparisons between two groups, Student's t-test was employed if the data exhibited normal distribution; otherwise, a nonparametric test was utilized. For comparisons among more than two groups, Analysis of Variance (ANOVA) was used for normally distributed data, while suitable nonparametric tests were applied for data not meeting normality assumptions, with the significance level set at $p < 0.05$. Single-cell RNA sequencing data analysis was performed using R software version 4.2.1, incorporating quality control, normalization, and differential gene expression identification through specialized R packages designed for scRNA-seq analysis.

## Results

### Unveiling the complexity of immune cell dynamics

Single-cell RNA sequencing has been used to delineate the intricacies of immune cell interplay, capturing the transcriptional heterogeneity of discrete immune populations. Dimensionality reduction methodologies, specifically t-SNE and UMAP, have facilitated the visualization of distinct cellular assemblages, encompassing B cells, NK cells, monocytes, and, notably, $CD8^{+}$T cells and M2 macrophages (Supplementary Figs. 1–3). Each aggregation represents a unique transcriptional signature, highlighting the intricate complexity of the immune cellular environment (Fig. 1A and B). The pseudotime trajectory analysis, which was applied to single-cell sequencing data, organizes cells along a two-dimensional continuum defined by Component 1 and Component 2. A gradient from darker to lighter hues indicates the progression through pseudotime, with the darker tones representing the beginning and the the lighter tones

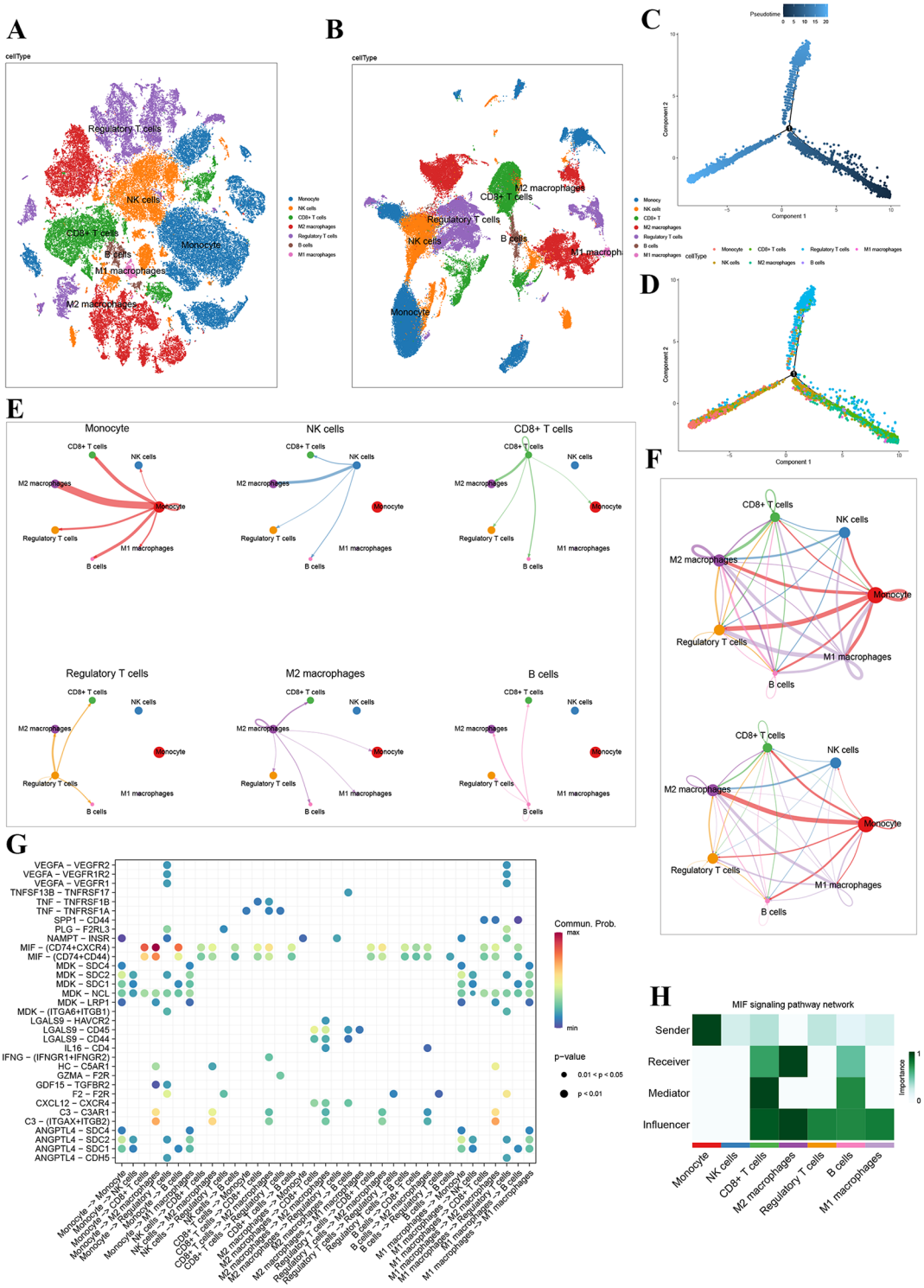
A
cellType
Regulatory T cells
NK cells
CD8+ T cells
Monocyte
B cells
M1 macrophages
M2 macrophages
Monocyte
NK cells
CD8+ T cells
M2 macrophages
Regulatory T cells
B cells
M1 macrophages
B
cellType
M2 macrophages
CD8+ T cells
Regulatory T cells
NK cells
B cells
Monocyte
C
Pseudotime
Component 1
Component 2
cellType
Monocyte
NK cells
CD8+ T cells
M2 macrophages
Regulatory T cells
B cells
M1 macrophages
D
Component 1
Component 2
E
Monocyte
NK cells
CD8+ T cells
Regulatory T cells
M2 macrophages
B cells
F
CD8+ T cells
NK cells
M2 macrophages
Monocyte
Regulatory T cells
M1 macrophages
B cells
G
VEGFA – VEGFR2
VEGFA – VEGFR1R2
VEGFA – VEGFR1
TNFSF13B – TNFRSF17
TNF – TNFRSF1B
TNF – TNFRSF1A
SPP1 – CD44
PLG – F2RL3
NAMPT – INSR
MIF – (CD74+CXCR4)
MIF – (CD74+CD44)
MDK – SDC4
MDK – SDC2
MDK – SDC1
MDK – NCL
MDK – LRP1
MDK – (ITGA6+ITGB1)
LGALS9 – HAVCR2
LGALS9 – CD45
LGALS9 – CD44
IL16 – CD4
IFNG – (IFNGR1+IFNGR2)
HC – C5AR1
GZMA – F2R
GDF15 – TGFBR2
F2 – F2R
CXCL12 – CXCR4
C3 – C3AR1
C3 – (ITGAX+ITGB2)
ANGPTL4 – SDC4
ANGPTL4 – SDC2
ANGPTL4 – SDC1
ANGPTL4 – CDH5
Commun. Prob.
max
min
p-value
0.01 < p < 0.05
p < 0.01
H
MIF signaling pathway network
Sender
Receiver
Mediator
Influencer
Importance
Monocyte
NK cells
CD8+ T cells
M2 macrophages
Regulatory T cells
B cells
M1 macrophages

**Fig. 1** Comprehensive Immune Landscape Analysis and Signaling Pathway Communication. **A**) T-distributed Stochastic Neighbor Embedding (t-SNE) plot demonstrating the distribution of immune cell subsets in the tumor microenvironment. Each color represents a unique cell type, with annotations indicating predominant immune populations such as Regulatory T cells, NK cells, and various macrophage phenotypes. **B**) Uniform Manifold Approximation and Projection (UMAP) plot delineating cellular clusters and their inferred developmental trajectories. Key immune subsets are identified and labeled correspondingly. **C**) t-SNE plot highlighting the pseudo-temporal ordering of cells, with color gradation from dark to light representing the progression from early to late differentiation states. **D**) Pseudotime trajectory analysis of immune cells across the first two principal components, revealing discrete lineage commitment points and differentiation pathways. **E**) Cell-cell interaction network diagrams for select immune subsets, with arrows depicting the directionality of signaling interactions. Node size corresponds to the number of outgoing interactions (sender) and edge thickness represents the interaction strength. **F**) Global interaction network across multiple immune cell types, integrating the strength of bidirectional signaling communications. Dominant signaling pathways are emphasized with thicker, colored edges, while secondary interactions are represented by thinner lines. **G**) Dot plot matrix showing the cell-type-specific expression of key signaling ligands and their receptors. Dot size indicates the level of gene expression, while color intensity reflects the probability of intercellular communication mediated by the respective signaling axis. **H**) Heatmap of the Macrophage Inflammatory Factor (MIF) signaling pathway network, categorizing cell types as senders, receivers, mediators, and influencers based on their role in the signaling cascade. Color intensity denotes the relative contribution to the MIF pathway

represnting the subsequent stages (see Fig. 1C). The trajectory originates from a nodal point, which may indicate a progenitor or a naive state. Subsequent cellular divergence occurs along bifurcating paths, suggesting discrete differentiation or maturation processes. It is noteworthy that the distribution of $CD8^+$T cells aligns predominantly with the early phases of tumorigenesis, as evidenced by the trajectory analysis (see Fig. 1D). Our network interaction assays (Fig. 1E) show reciprocal signaling between $CD8^+$T cells and M2 macrophages, facilitated by a repertoire of signaling molecules and their cognate receptors. This establishes a crucial axis of regulation within the immune schema. An exhaustive network analysis (Fig. 1F) illustrates the centrality of $CD8^+$T cells and M2 macrophages within the immune signaling nexus This interaction map highlights the important roles these cell types play in modulating immune responses. A heatmap of ligand-receptor pairs (Fig. 1G) emphasizes the MIF signaling pathway as a key mediator of $CD8^+$T cell and M2 macrophage communication. This analysis reveals the extensive nature of their interaction, highlighting the essential role of MIF in corrdinating immune dynamics.

The MIF signaling pathway schematic highlights M2 macrophages and $CD8^+$T cells as the main actors. M2 macrophages are shown to be influential regulators within the pathway, while CD8 + T cells are highlighted as important responders to MIF signaling (Fig. 1H and Supplementary Fig. 4). This framework emphasizes the collaborative and crucial roles of M2 macrophages and $CD8^+$T cells in regulating the immune system.

## Effect of RFA on immune microenvironment of liver cancer in mice

Using the insights gained from our single-cell analysis of the tumor microenvironment's immune landscape, we established an in situ bimodal hepatic tumor model in mice (refer to Fig. 2). This model' enabled subsequent flow cytometric analyses of intrahepatic tumors that are not subjected to ablation. The study revealed trends of increased immune cell infiltration in the tumor microenvironment, including CD8 + T lymphocytes, CD4 + T lymphocytes, and macrophages (see Supplementary Fig. 5 for details). Conversely, a notable decrease in the presence of immunosuppressive populations, such as myeloid-derived suppressor cells (MDSCs) and dendritic cells, was observed (further elaboration in the Supplementary Fig. 5).

Furthermore, there was a noticeable increase in the infiltration of other immunosuppressive mesenchymal cells, such as MDSCs and macrophages, which also exhibited elevated PD-L1 expression, as detailed in the supplementary figure. These findings support the hypothesis that localized inflammatory responses induced by RFA can create a tumor-suppressive immune microenvironment. This highlights the complex interaction between therapeutic interventions and the immune system's crucial role in oncological management.

## T cell appears functionally exhausted at the late stage of RFA treatment

In our subsequent analysis of the antitumor immune response triggered by RFA, we investigated the dynamics of immune cell infiltration following the procedure. We quantified the infiltration of CD45 + leukocytes within tumor tissues after ablation. Our results showed a significant increase in the proportion of CD45 + immune cells in ablated tumors by day three post-RFA. This increase persisted, with a substantial rise in the CD45 + lymphocyte population by day six, suggesting that the infiltration was sustained over time (Supplementary Fig. 5). These findings underscore the persistence and amplification of the RFA-induced inflammatory response, extending into the period of accelerated tumor growth. Notably, the density of cytotoxic CD8 + T lymphocytes was significantly higher on day six post-ablation compared to day three (Fig. 3A), indicating enhanced adaptive immune surveillance that could improve antitumor efficacy during the critical phase of tumor regrowth following ablation. On day three post-ablation, CD4 + T lymphocytes expressing TNF-α and

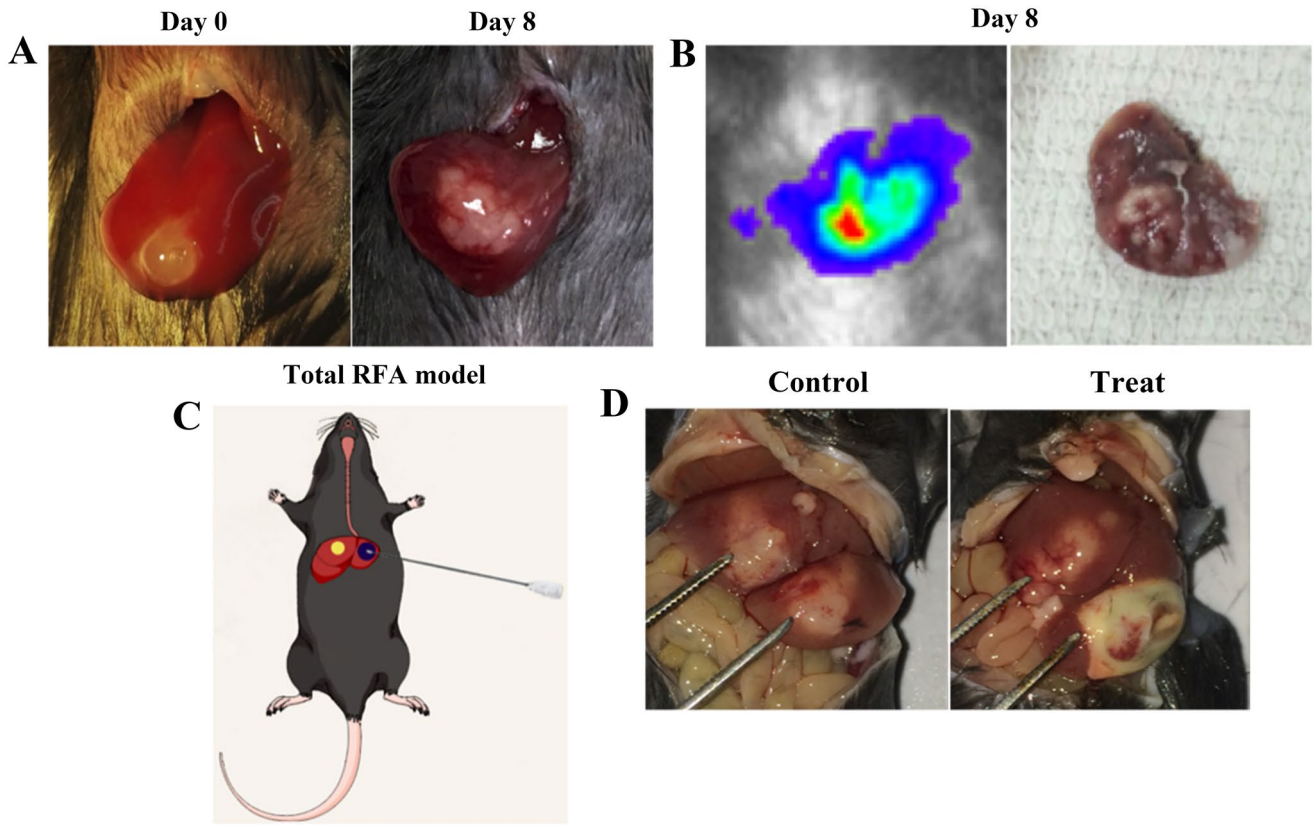


**Fig. 2** Murine Model Evaluation of Tumor Development and Radiofrequency Ablation (RFA) Efficacy. **A**) Longitudinal visual comparison of tumor development in a rodent model, demonstrating the initial appearance of the hepatic tumor at Day 0 and its size increase by Day 8. **B**) Left: Thermographic image illustrating the distribution of heat during RFA treatment on Day 8, with the color intensity indicating temperature variation. Right: Gross morphology of the excised hepatic tumor post-RFA intervention, showing the extent of tissue necrosis. **C**) Illustrative diagram depicting the rodent subject with the total RFA model setup, indicating the precise application of the RFA probe to the targeted hepatic tumor. **D**) Intraoperative comparison between the control (untreated) and treated groups within the study. The control display reveals a hepatic tumor without RFA intervention, and the treated image demonstrates the effects post-RFA, including areas of ablation and tissue alteration

IFN-γ were significantly higher in the RFA group compared to the control. By day six, these levels decreased, with no significant difference between groups (Fig. 3B).

To assess the antitumor activity of the infiltrating T cells, we performed flow cytometry to measure the production of IFN-γ and TNF-α by CD8 + T cells and CD4 + T cells. Three days after the ablation procedure, the proportions of IFN-γ + and TNF-α + CD8 + tumor-infiltrating lymphocytes (TILs), as well as IFN-γ + and TNF-α + CD4 + TILs, were significantly higher in the treatment group—approximately 2–3 times greater than those in the control group. However, by day six post-ablation, there was a marked reduction in the proportions of both CD8 + and CD4 + TILs in the ablation group. Furthermore, the levels of IFN-γ + CD8 + TILs and TNF-α + CD4 + TILs had returned to levels comparable to the control group (Fig. 3C-D). These findings suggest that the functionality of activated T cells diminishes in the later stages following RFA, indicating the onset of immunosuppression.

## Synergistic effects of ablation and anti-PD-L1 therapy on distant tumors and survival in mice

To assess whether the combination of RFA and anti-PD-L1 antibody therapy could produce synergistic antitumor effects, we developed a dual tumor model in mice. This model included both in situ liver tumors and subcutaneous tumors on the dorsum. After 7–8 days post-tumor implantation, which was confirmed by fluorescence imaging (tumors measuring 0.8–1.0 cm in diameter), we performed complete ablation was performed on the hepatic tumors (Fig. 4A). The mice were randomly allocated mice into four groups: an untreated control group ($n = 7$), a group treated with RFA alone ($n = 7$), a group treated with anti-PD-L1 antibody alone ($n = 8$), and a group treated with combined RFA and a-PD-L1 antibody therapy ($n = 8$). Details on the treatment regimen for each group are provieded in Fig. 4A-B. The comparative analysis revealed that, in contrast to the RFA and a-PD-L1 groups, mice in the combined treatment

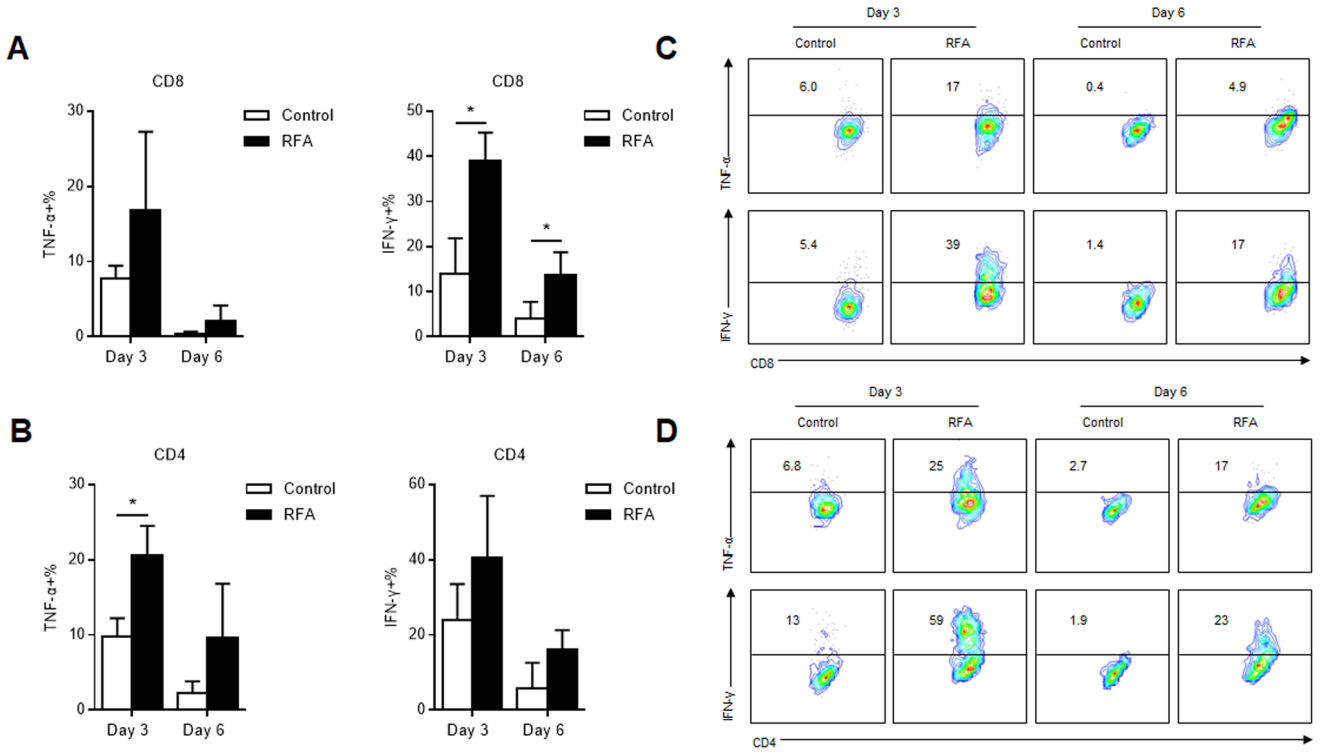


**Fig. 3** Immune Response Characterization Following Radiofrequency Ablation (RFA) in a Rodent Model. **A**) Bar graphs depicting the percentage of CD8 + T cells expressing TNF-α and IFN-γ at Day 3 and Day 6 post-RFA compared to the control group. There is a marked increase in IFN-γ expression by Day 6 in the RFA-treated group, indicating an enhanced Th1 response (*$p < 0.05$; statistical test: Two-way ANOVA). **B**) Similar bar graphs for CD4 + T cells showing a significant rise in TNF-α expression by Day 3 in the RFA group, suggesting early activation of the Th1 subset (*$p < 0.05$; statistical test: Two-way ANOVA). **C**) Flow cytometry plots illustrating the expression of TNF-α and IFN-γ in CD8 + T cells at Day 3 and Day 6. The RFA group shows an elevated proportion of cytokine-expressing cells, particularly for IFN-γ at Day 6. **D**) Flow cytometry analysis for CD4 + T cells with corresponding expression patterns for TNF-α and IFN-γ. A clear shift towards higher IFN-γ expression is observed in the RFA group at Day 6

group exhibited slower tumor growth and smaller dorsal subcutaneous tumor volumes (Fig. 4C-D, $p > 0.05$, indicating no significant difference though). The median survival times for mice for the four groups were 6.3, 7.5, 16, and 30 days, respectively. The combination treatment group had a significantly longer survival time ($p < 0.05$, Fig. 4E). The RFA group, a-PD-L1 group, and the combination group all exhibited temporary tumor growth inhibition during treatment. However, this antitumor effect decreased after treatment, leading to accelerated tumor growth. In contrast, mice in the RFA combined with a-PD-L1 treatment groups 1 and 2 demonstrated progressive tumor regression, with a reduction in tumor volume exceeding 90% (refer to Fig. 4F-I).

## Enhanced tumor immune microenvironment and T cells efficacy with combined ablation and anti-PD-L1 therapy

To determine whether anti-PD-L1 treatment could reverse the suppressive tumor microenvironment induced by RFA, we analyzed the subcutaneous tumors of four treatment groups of tumor-bearing mice using flow cytometry. Our analysis focused on the changes in the proportions of mononuclear cell populations, including Tregs ($CD4^+FoxP3^+$ regulatory T cells), macrophages ($CD11b^+F4/80^+$), myeloid-derived suppressor cells (MDSCs, $CD11b^+Gr1^+$), and dendritic cells (DCs, $CD11c^+$).

After post-combined anti-PD-L1 treatment, there was an observed increase in the infiltration of antigen-presenting cells, including macrophages and DCs, was observed in the subcutaneous tumors. The infiltration of macrophages in the anti-PD-L1 group was statistically significant when compared with the RFA group. Furthermore, the recruitment of DC cells in the combination therapy group also showed a significant difference compared to the other groups (see Fig. 5A, B). Analysis of PD-L1 expression across different cell populations revealed that tumor cells exhibit lower PD-L1 expression, while MDSCs exhibit the highest expression rate (refer to Fig. 5C). Treatment with anti-PD-L1 significantly reduced PD-L1 expression intensity in various immune cells, although this effect was not pronounced in the combined treatment (refer to Fig. 5D). These results collectively suggest that combined anti-PD-L1 blockade

therapy can positively modulate the immune microenvironment balance in distant tumors post-ablation.

Flow cytometry analysis revealed that the combined therapies regimen resulted in a significant increase in $CD8^+$ tumor-infiltrating lymphocytes (TILs) with the combined therapies group compared to only one form of treatment. This increase led to a marked boost in the secretion of cytotoxic cytokines IFN-γ and TNF-α (Fig. 6A). Although $CD4^+$TILs did not vary significantly across the cohorts, the combined treatment group exhibited a substantial increase in IFN-γ and TNF-α levels compared to both the single-treatment groups and the control group. This suggests that effector T cells have an enhanced anti-tumor efficacy (Fig. 6B). On the eleventh day after treatment, a significant decrease in Treg cell presence was observed in the cohorts treated with anti-PD-L1 alone and in synergy with RFA, in contrast to the group treated exclusively with RFA (srefer to Fig. 6C). It is noteworthy that the $CD8^+$/Treg ratio was significantly higher in the combined therapy group compared to all other groups (refer to Fig. 6D). Furthermore, the analysis suggests that anti-PD-L1 therapy inhibits the growth and movement of MDSCs in subcutaneous tumors. The combination therapy group showed a statistically significant difference from the untreated group.

## Discussion

Hepatocellular carcinoma (HCC) is known for its complex etiology and often presents at an advanced stage, resulting in a staggeringly low five-year survival rate. Therefore, innovative and more effective therapeutic approaches are urgently needed.

To gain a deeper understanding of the tumor microenvironment in HCC, we performed a single-cell analysis of HCC samples using publicly available datasets. Thirteen HCC samples were carefully selected for detailed investigation. Following a rigorous cell filtration process, we identified various cell types within the HCC microenvironment based on specific markers, allowing us to distinguish populations such as CD8 + T cells, regulatory T cells (Tregs), M1 and M2 macrophages, and CD4 + memory T cells. To explore the relationship between these cells and their evolution during the initiation and progression of HCC, we conducted a cell trajectory analysis. This analysis revealed a significant increase in CD8 + T cells in the early stages of HCC. While CD8 + T cells are typically known for their tumor-killing ability, their increased presence did not halt tumor progression, leading us to hypothesize that these CD8 + T cells may become exhausted. This exhaustion could contribute to the continued progression of HCC, suggesting a complex interplay between the immune response and tumor development.

The basis of the body's anti-tumor response is mainly mediated by T cell-led immune responses [20]. The efficacy of the immune response against tumors is determined by the number and functional state of these cells infiltrating the tumor microenvironment [21]. Tumor-infiltrating lymphocytes (TILs) are closely associated with type 1 interferon (IFN) secretion [22, 23]. Their presence has been shown to be a favorable prognostic factor in many cancers [24, 25]. Studies have shown that, the tumor microenvironment contains various T cell subsets including regulatory T cells (Tregs) [26], exhausted T cells, and anergic T cells [27], in addition to $CD8^+$ cytotoxic T lymphocytes (CTLs). These subsets can suppress the tumor immune response and promote tumor invasion and metastasis [28–30].

Percutaneous RFA is a widely accepted alternative treatment method for patients with liver tumors, due to its safety and low rate of major complications. RFA treatment is believed to cause extensive cell necrosis, releasing cellular debris that serves as a source of tumor antigens. This triggers an immune response against the tumor, including the activation of immune and cryptic antigens that induce tumor-specific T cell responses. However, there are relatively few reports on the overall impact of ablative therapy on the body's immune status. Therefore, we are investigating the effects of RFA on the body's immune function, specifically the changes in the immune microenvironment such as macrophages and exhausted T cells after RFA, and monitoring the expression of PD-L1 after ablation.

Compared to typical liver cancer tissues, there was a significant increase in PD-L1 expression in residual liver cancer tissues after incomplete RFA [31]. This suggests that RFA-induced local microenvironmental changes may lead to the upregulation of PD-L1 expression. we further investigated the changes in the immune microenvironment after ablation and successfully established a dual tumor model in mice. In this model, we observed that non-ablative liver tumors exhibited an increase in immune cell infiltration within the tumor tissue. This infiltration was predominantly characterized by a higher presence of macrophages, $CD8^+$T cells, and $CD4^+$T cells, indicating a significant change in the immune landscape after RFA treatment. Interestingly, tumor regression at non-irradiated distant tumor sites in some circumstances, which is called the "abscopal effect" [32, 33]. we assume that the upregulation of macrophages, $CD8^+$T cells, and $CD4^+$T cells is due to abscopal effect change immunosuppression to immune stimulation. Abscopal effect as a stimulator of immune system in combination with immunotherapy. Increase in antigen presentation following higher ratio of immunologic cell death within TME can amplify anti-tumor immunity [32]. By leveraging this principle, the study aims to elucidate the mechanisms by which RFA influences immune responses in non-targeted

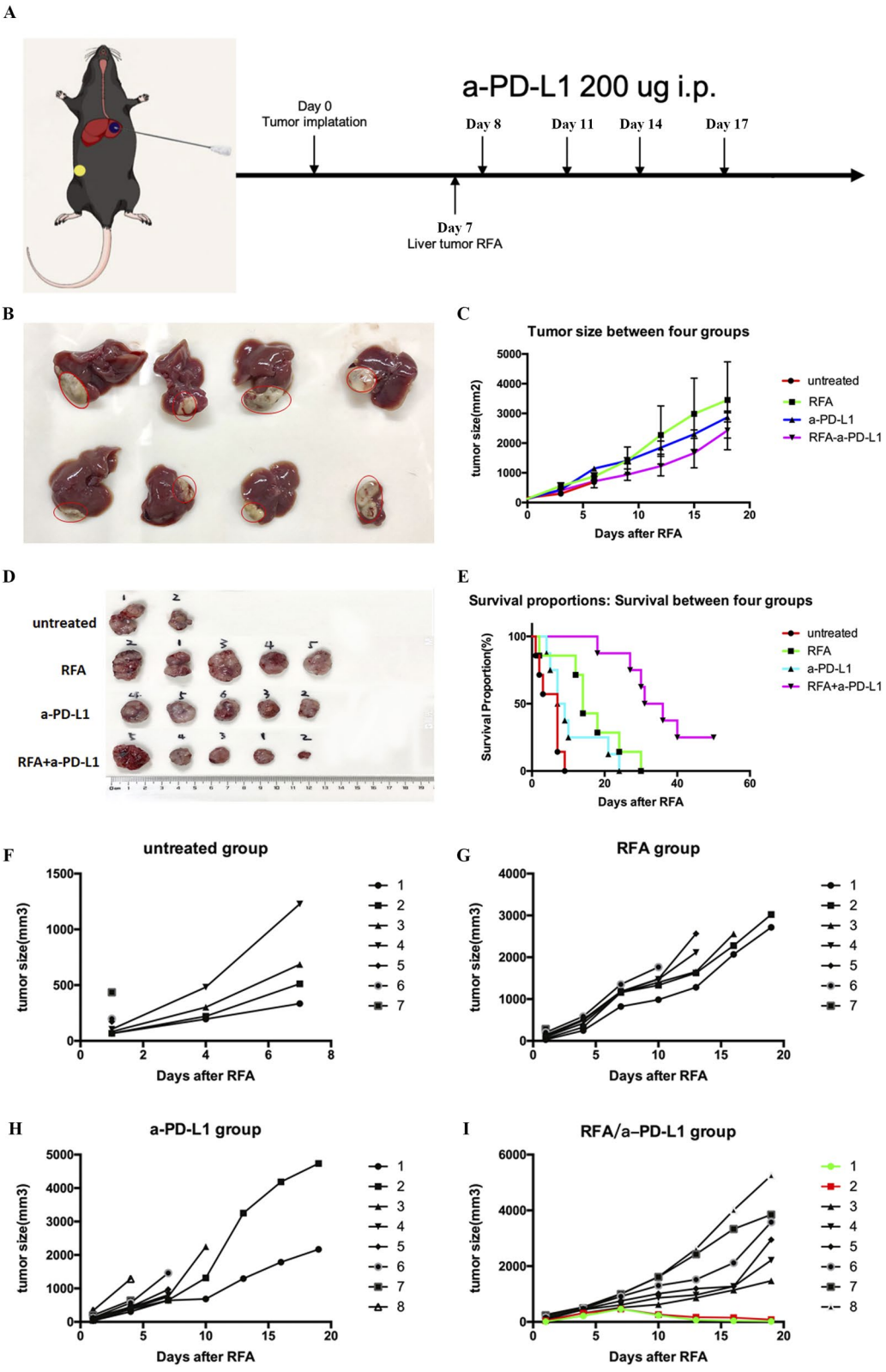
A
a-PD-L1 200 ug i.p.
Day 0
Tumor implatation
Day 8
Day 11
Day 14
Day 17
Day 7
Liver tumor RFA
B
C
Tumor size between four groups
tumor size(mm2)
Days after RFA
untreated
RFA
a-PD-L1
RFA-a-PD-L1
D
untreated
RFA
a-PD-L1
RFA+a-PD-L1
E
Survival proportions: Survival between four groups
Survival Proportion(%)
Days after RFA
untreated
RFA
a-PD-L1
RFA+a-PD-L1
F
untreated group
tumor size(mm3)
Days after RFA
G
RFA group
tumor size(mm3)
Days after RFA
H
a-PD-L1 group
tumor size(mm3)
Days after RFA
I
RFA/a-PD-L1 group
tumor size(mm3)
Days after RFA

**Fig. 4** Therapeutic Efficacy of Radiofrequency Ablation (RFA) Combined with Anti-PD-L1 Immunotherapy. **A**) Tumor cells were implanted in the liver on Day 0. Radiofrequency ablation (RFA) of the liver tumor was performed on Day 7. Anti-PD-L1 (200 μg) was administered intraperitoneally (i.p.) on Days 8, 11, 14, and 17 **B**) Collection of excised livers depicting the variability in tumor burden post-intervention. **C**) Line graph presenting tumor size quantification across four experimental groups: untreated, RFA alone, a-PD-L1 monotherapy, and RFA combined with a-PD-L1. The combination therapy group shows a significant reduction in tumor growth over time. **D**) Representative liver specimens from each treatment group showcasing comparative outcomes. Notable tumor regression is observed in the RFA combined with a-PD-L1 cohort. **E**) Kaplan-Meier survival curves for the four groups, illustrating enhanced survival benefit in the RFA plus a-PD-L1 treatment group (statistical test: Log-rank (Mantel-Cox) test). **F-I**) Individual tumor growth kinetics within each group, demonstrating the heterogeneity of response. The RFA/a-PD-L1 group (**I**) exhibits a marked suppression of tumor progression compared to other treatments

tumors, thereby contributing to a more comprehensive understanding of tumor-immune dynamics and informing the development of novel therapeutic strategies.

The PD-L1 expression in the tissue outside the ablation site showed an increasing trend, primarily in tumor cells. Inhibitory stromal cells, such as MDSCs and macrophages, also showed significant increases in infiltration and predominantly expressed PD-L1. These findings suggest that RFA-mediated local inflammatory responses can induce the formation of a suppressive tumor immune microenvironment.

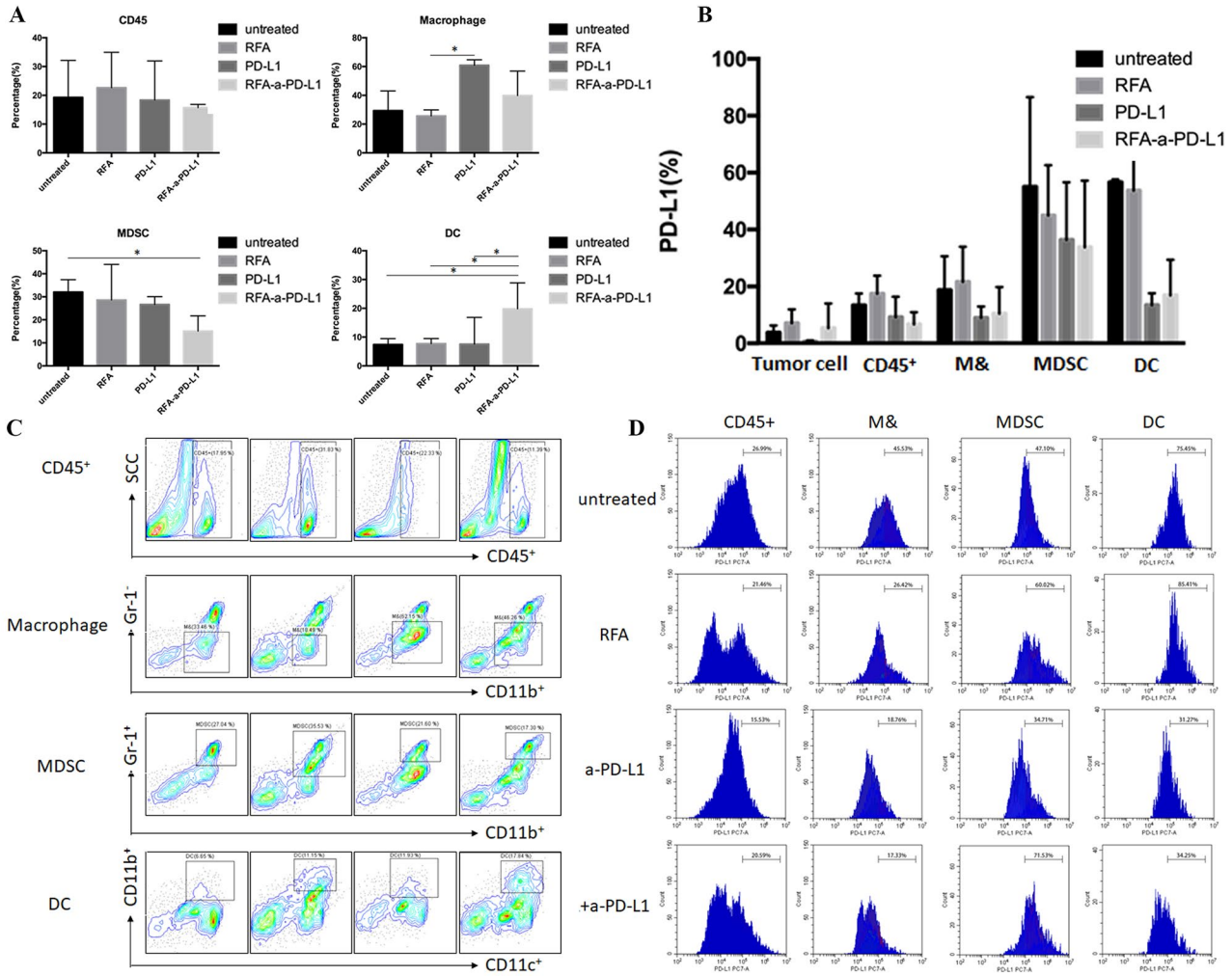


**Fig. 5** Immunomodulatory Effects of RFA and Anti-PD-L1 Therapy on Tumor Microenvironment **A**) Bar graphs representing the frequency of CD45 + leukocytes, macrophages, MDSCs, and DCs in untreated, RFA, anti-PD-L1 (a-PD-L1), and combination therapy (RFA + a-PD-L1) groups, indicating alterations in immune cell populations upon different treatments(statistical test: Two-way ANOVA). **B**) The expression of PD-L1 on tumor cells, CD45 + leukocytes, macrophages (M&), MDSCs, and DCs across the same treatment groups, with significant upregulation noted in certain populations post-treatment, especially with the combination therapy(statistical test: Two-way ANOVA). **C**) Flow cytometry contour plots illustrating the gating strategy for immune cell populations and their subsets within the tumor microenvironment, highlighting differences in cell frequency and phenotype post-treatment. **D**) Histograms of PD-L1 expression on CD45 + leukocytes, macrophages (M&), MDSCs, and DCs for each treatment group (untreated, RFA, a-PD-L1, RFA + a-PD-L1), demonstrating the impact of RFA and anti-PD-L1 therapy on PD-L1 levels within these immune cell subsets

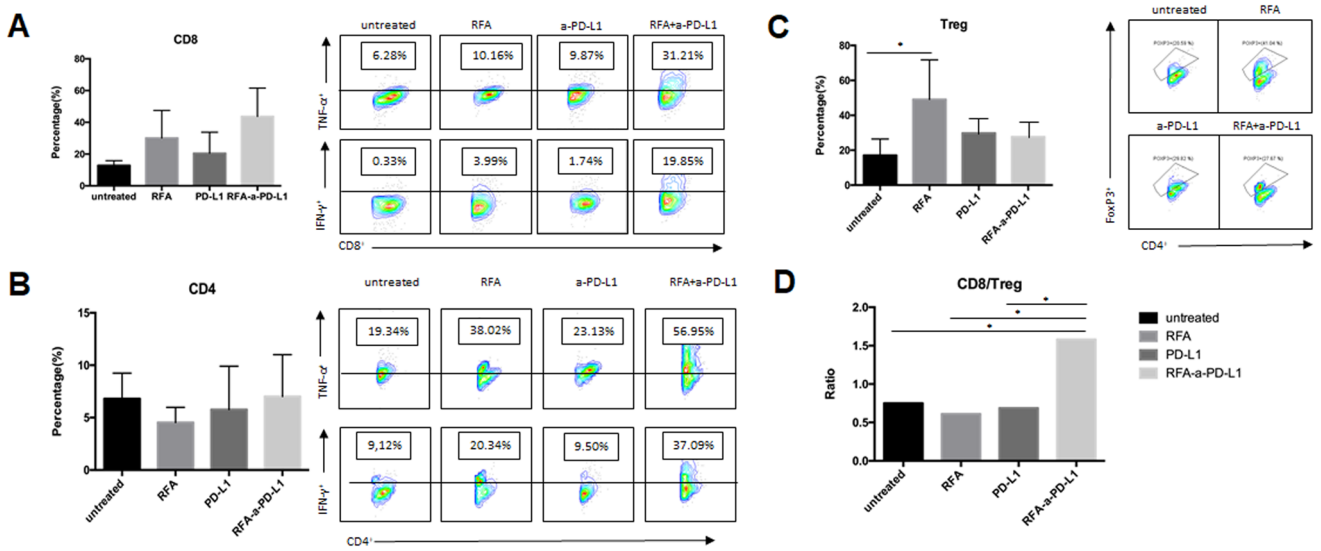


**Fig. 6** Functional and Regulatory T Cell Profiles Following RFA and PD-L1 Inhibition **A**) Bar graphs show the percentages of TNF-α + and IFN-γ + among CD8 + T cells, with an adjacent set of flow cytometry contour plots for each treatment group. Enhanced cytokine expression is observed post-RFA and PD-L1 inhibition, with a notable synergistic increase in the dual-treated cohort(statistical test: Two-way ANOVA). **B**) For CD4 + T cells, the data display a similar trend in cytokine production as CD8 + T cells, with the RFA + a-PD-L1 group exhibiting the most substantial elevation in TNF-α and IFN-γ expression (statistical test: Two-way ANOVA). **C**) The proportion of T regulatory cells (CD4 + FoxP3+) is quantified, showing a decrease in Treg frequency following combined RFA and anti-PD-L1 therapy, as visualized in the corresponding flow cytometry plots (statistical test: Two-way ANOVA). **D**) The ratio of CD8 + T cells to Tregs is graphed, indicating an increased ratio in the RFA and RFA + a-PD-L1 groups, suggestive of an immune environment more conducive to anti-tumor activity (statistical test: Two-way ANOVA)

To evaluate the anti-tumor capabilities of infiltrating T cells, we analyzed the abiliy of $CD8^+$ and $CD4^+$T cells to secrete IFN-γ and TNF-α. Three days after ablation, a significant increase in both IFN-$\gamma^+$ and TNF-$\alpha^+$ was observed among $CD8^+$ tumor-infiltrating lymphocytes, as well as in the IFN-$\gamma^+$ and TNF-$\alpha^+CD4^+$TILs within the treatment group. This finding highlights a significant improvement in the immune response after treatment. Interestingly, the ratio of lymphocyte infiltration in tumor tissues, especially $CD8^+$T cells, significantly increased in the post-ablation period compared to the control group. However, their secretion of tumor-killing cytokines IFN-γ and TNF-α showed a decreasing trend, similar to the control group levels, suggesting that most T cells experienced functional exhaustion and were unable to sustain their anti-tumor effects. Notably, this finding highlights the importance of considering the functional status of T cells in cancer immunotherapy.

Tumors may utilize the expression of co-inhibitory PD-L1 molecules to bind with PD-1 on the surface of T cells. This can lead to effector T cell exhaustion, suppressing T cell-mediated immune responses, promoting immune escape of tumor cells. This indicates a poor prognosis. PD-L1 appears to play a bridging role in mediating the transition from 'immune activation' to 'immune tolerance' in tumors [34–36]. Our research indicates that PD-L1 expression is significantly upregulated in tumor tissues after RFA treatment, which may be the cause of tumor immune escape after treatment.

Studies have shown that combining PD-1 blockade with RFA can significantly improve outcomes for patients with recurrent HCC. This combined therapy appears to reduce local tumor recurrence and enhance overall survival compared to RFA alone [37].

PD-1 is expressed on T cells and interacts with its ligand PD-L1, which can be expressed on both tumor cells and immune cells within the tumor microenvironment. This interaction plays a crucial role in tumor immune evasion. By blocking PD-1/PD-L1, the immune response against tumor cells is reactivated, potentially leading to improved control of tumor growth and reduced recurrence rates [38].

To test the hypothesis that RFA combined with anti-PD-L1 tumor treatment could have synergistic anti-tumor effects, we established a dual tumor model in mice with in situ liver tumor and subcutaneous back tumor. Compared to the RFA or a-PD-L1 alone group, the combination group exhibited relatively slower tumor growth and smaller tumor volume in subcutaneous back tumors. Additionally, their survival time was significantly prolonged compared with other treatment groups. Our results suggest that anti-PD-L1 therapy may counteract the suppressive tumor microenvironment induced by RFA, our results revealed a remarkable observation. After ablation treatment, infiltration of Treg cells infiltration was significantly reduced in both the

anti-PD-L1 group and the combination group compared to the RFA alone group. This indicates a potential therapeutic synergy in alleviating tumor-induced immune suppression when combining RFA with anti-PD-L1 treatment. The combination treatment group exhibited a significantly higher $CD8^+$/Treg ratio compared to other treatment groups, suggesting that the combined anti-PD-L1 blockade treatment can enhance the immune microenvironment balance in distant tumors after ablation. Our subsequent analysis of tumor-infiltrating lymphocytes revealed a crucial finding. The combined treatment group demonstrated a significant increase in the $CD8^+$TILs infiltration compared to the single treatment groups. This study found that the combination of RFA with anti-PD-L1 therapy significantly increased the ability of T cells to secrete the cytotoxic cytokines IFN-γ and TNF-α. These results suggest that the combination of RFA with anti-PD-L1 therapy not only improves the tumor immune microenvironment, but also enhances the anti-tumor efficacy of the infiltrating T cells. These findings highlight the potential of combining RFA with anti-PD-L1 therapy as a more effective strategy to combat tumor progression.

## Conclusion

Our study on HCC provides critical insights into the tumor microenvironment, highlighting the dual role of immune cells and the impact of RFA combined with anti-PD-L1 therapy. We found that $CD8^+$T cells initially increase and kill the tumor, but become exhausted over time, underscoring the complex interplay between tumor progression and immune response. Our findings demonstrate that RFA induces PD-L1 expression, promoting immune escape. Combining RFA with anti-PD-L1 treatment can significantly enhance immune response, reduce Treg cell infiltration, and improve the CD8+/Treg ratio, suggesting a potent strategy to combat HCC. This suggests a potent strategy for combating HCC and improving therapeutic outcomes by harnessing the immune system's capacity to fight cancer.

**Supplementary Information** The online version contains supplementary material available at https://doi.org/10.1007/s10495-024-02019-3.

**Acknowledgements** We sincerely thank Dr. Juncheng Wang (Sun Yat-sen University Cancer Center, China) for providing experimental technical guidance for this study.

**Author contributions** Conception and design: Jiaming Lai. Acquisition of data: Jiahua Liang and Mingjian Ma. Analysis and curation of data: Jiahua Liang, Wei Feng and Jiancong Chen. Drafting the article: Jiahua Liang. Critically revising the article: all authors. Study supervision: Jiancong Chen. All authors read and approved the final manuscript.

**Funding** This work was supported by the Basic and Applied Basic Research Fund of Guangdong Province (2020A1515110485).

**Data availability** No datasets were generated or analysed during the current study.

## Declarations

**Ethical approval** The study was also in accordance with the Helsinki Declaration and approved by the Ethics Committee of the First Affiliated Hospital of Sun Yat-sen University [No. [2024]459]. Written informed consents were obtained from all patients.

**Consent for publication** Not applicable.

**Competing interests** The authors declare no competing interests.



## References

1. Singal AG, Kanwal F, Llovet JM (2023) Global trends in hepatocellular carcinoma epidemiology: implications for screening, prevention and therapy. Nat Reviews Clin Oncol 20:864–884. https://doi.org/10.1038/s41571-023-00825-3
2. Qi X, Yang M, Ma L et al (2020) Synergizing sunitinib and radiofrequency ablation to treat hepatocellular cancer by triggering the antitumor immune response. J Immunotherapy cancer 8. https://doi.org/10.1136/jitc-2020-001038
3. Deng Q, He M, Fu C, Feng K, Ma K, Zhang L (2022) Radiofrequency ablation in the treatment of hepatocellular carcinoma. Int J Hyperthermia: Official J Eur Soc Hyperthermic Oncol North Am Hyperth Group 39:1052–1063. https://doi.org/10.1080/02656736.2022.2059581
4. Dumolard L, Ghelfi J, Roth G, Decaens T, Macek Jilkova Z (2020) Percutaneous ablation-Induced Immunomodulation in Hepatocellular Carcinoma. Int J Mol Sci 21. https://doi.org/10.3390/ijms21124398
5. Mizukoshi E, Yamashita T, Arai K et al (2013) Enhancement of tumor-associated antigen-specific T cell responses by radiofrequency ablation of hepatocellular carcinoma. Hepatology (Baltimore MD) 57:1448–1457. https://doi.org/10.1002/hep.26153
6. Li J, Xuan S, Dong P et al (2023) Immunotherapy of hepatocellular carcinoma: recent progress and new strategy. Front Immunol 14:1192506. https://doi.org/10.3389/fimmu.2023.1192506
7. Janopaul-Naylor JR, Shen Y, Qian DC, Buchwald ZS (2021) The Abscopal Effect: A Review of Pre-Clinical and Clinical Advances. 22:11061

8. Tracz JA, Donnelly BM, Ngu S, Vojnic M, Wernicke AG, D'Amico RS (2023) The abscopal effect: inducing immunogenicity in the treatment of brain metastases secondary to lung cancer and melanoma. J Neurooncol 163:1–14. https://doi.org/10.1007/s11060-023-04312-8
9. Li T, Li B, Sara A et al (2019) Docking protein-1 promotes inflammatory macrophage signaling in gastric cancer. Oncoimmunology 8:e1649961. https://doi.org/10.1080/2162402x.2019.1649961
10. Zeng X, Liao G, Li S et al (2023) Eliminating METTL1-mediated accumulation of PMN-MDSCs prevents hepatocellular carcinoma recurrence after radiofrequency ablation. Hepatology (Baltimore MD) 77:1122–1138. https://doi.org/10.1002/hep.32585
11. Chen S, Zeng X, Su T et al (2022) Combinatory local ablation and immunotherapies for hepatocellular carcinoma: Rationale, efficacy, and perspective. Front Immunol 13:1033000. https://doi.org/10.3389/fimmu.2022.1033000
12. Wang D, Luo J, Tao Y (2023) Tumor–stroma ratio predicts prognosis and PD-L1 expression in hepatocellular carcinoma. BMC Cancer 23:434. https://doi.org/10.1186/s12885-023-10859-6
13. Shi ZR, Duan YX, Cui F et al (2023) Integrated proteogenomic characterization reveals an imbalanced hepatocellular carcinoma microenvironment after incomplete radiofrequency ablation. J Experimental Clin cancer Research: CR 42:133. https://doi.org/10.1186/s13046-023-02716-y
14. Zhao T, Wei P, Zhang C et al (2024) Nifuroxazide suppresses PD-L1 expression and enhances the efficacy of radiotherapy in hepatocellular carcinoma. eLife 12. https://doi.org/10.7554/eLife.90911
15. Shinchi Y, Ishizuka S, Komohara Y et al (2022) The expression of PD-1 ligand 1 on macrophages and its clinical impacts and mechanisms in lung adenocarcinoma. Cancer Immunol Immunotherapy: CII 71:2645–2661. https://doi.org/10.1007/s00262-022-03187-4
16. Caputo AT, Eder OM, Bereznakova H et al (2021) Structure-guided selection of puromycin N-acetyltransferase mutants with enhanced selection stringency for deriving mammalian cell lines expressing recombinant proteins. Sci Rep 11:5247. https://doi.org/10.1038/s41598-021-84551-9
17. Cossarizza A, Chang HD, Radbruch A et al (2021) Guidelines for the use of flow cytometry and cell sorting in immunological studies (third edition). Eur J Immunol 51:2708–3145. https://doi.org/10.1002/eji.202170126
18. Perfetto SP, Ambrozak D, Nguyen R, Chattopadhyay PK, Roederer M (2012) Quality assurance for polychromatic flow cytometry using a suite of calibration beads. Nat Protoc 7:2067–2079. https://doi.org/10.1038/nprot.2012.126
19. Herzenberg LA, Tung J, Moore WA, Herzenberg LA, Parks DR (2006) Interpreting flow cytometry data: a guide for the perplexed. Nat Immunol 7:681–685. https://doi.org/10.1038/ni0706-681
20. Levine AG, Mendoza A, Hemmers S et al (2017) Stability and function of regulatory T cells expressing the transcription factor T-bet. Nature 546:421–425. https://doi.org/10.1038/nature22360
21. Fuertes MB, Kacha AK, Kline J et al (2011) Host type I IFN signals are required for antitumor CD8 + T cell responses through CD8{alpha}+ dendritic cells. J Exp Med 208:2005–2016. https://doi.org/10.1084/jem.20101159
22. Diamond MS, Kinder M, Matsushita H et al (2011) Type I interferon is selectively required by dendritic cells for immune rejection of tumors. J Exp Med 208:1989–2003. https://doi.org/10.1084/jem.20101158
23. Bochtler P, Kröger A, Schirmbeck R, Reimann J (2008) Type I IFN-induced, NKT cell-mediated negative control of CD8 T cell priming by dendritic cells. J Immunol (Baltimore Md: 1950) 181:1633–1643. https://doi.org/10.4049/jimmunol.181.3.1633
24. Tanaka F, Hashimoto W, Okamura H, Robbins PD, Lotze MT, Tahara H (2000) Rapid generation of potent and tumor-specific cytotoxic T lymphocytes by interleukin 18 using dendritic cells and natural killer cells. Cancer Res 60:4838–4844
25. Barbi J, Pardoll D, Pan F (2014) Treg functional stability and its responsiveness to the microenvironment. Immunol Rev 259:115–139. https://doi.org/10.1111/imr.12172
26. Maeda Y, Nishikawa H, Sugiyama D et al (2014) Detection of self-reactive $CD8^+$ T cells with an anergic phenotype in healthy individuals. Sci (New York NY) 346:1536–1540. https://doi.org/10.1126/science.aaa1292
27. Kamphorst AO, Wieland A, Nasti T et al (2017) Rescue of exhausted CD8 T cells by PD-1-targeted therapies is CD28-dependent. Sci (New York NY) 355:1423–1427. https://doi.org/10.1126/science.aaf0683
28. Fujii S, Shimizu K, Hemmi H, Steinman RM (2007) Innate Valpha14(+) natural killer T cells mature dendritic cells, leading to strong adaptive immunity. Immunol Rev 220:183–198. https://doi.org/10.1111/j.1600-065X.2007.00561.x
29. Fujii S (2008) Exploiting dendritic cells and natural killer T cells in immunotherapy against malignancies. Trends Immunol 29:242–249. https://doi.org/10.1016/j.it.2008.02.002
30. Oh BY, Hong HK, Lee WY, Cho YB (2017) Animal models of colorectal cancer with liver metastasis. Cancer Lett 387:114–120. https://doi.org/10.1016/j.canlet.2016.01.048
31. Liu J, Li X, Chen J et al (2024) Targeting SUMOylation with an injectable nanocomposite hydrogel to optimize radiofrequency ablation therapy for hepatocellular carcinoma. J Nanobiotechnol 22:338. https://doi.org/10.1186/s12951-024-02579-1
32. Ashrafizadeh M, Farhood B, Eleojo Musa A, Taeb S, Rezaeyan A, Najafi M (2020) Abscopal effect in radioimmunotherapy. Int Immunopharmacol 85:106663. https://doi.org/10.1016/j.intimp.2020.106663
33. Zhang Z, Liu X, Chen D, Yu J (2022) Radiotherapy combined with immunotherapy: the dawn of cancer treatment. Signal Transduct Target Therapy 7:258. https://doi.org/10.1038/s41392-022-01102-y
34. Yamaguchi H, Hsu JM, Yang WH, Hung MC (2022) Mechanisms regulating PD-L1 expression in cancers and associated opportunities for novel small-molecule therapeutics. Nat Reviews Clin Oncol 19:287–305. https://doi.org/10.1038/s41571-022-00601-9
35. Chen S, Crabill GA, Pritchard TS et al (2019) Mechanisms regulating PD-L1 expression on tumor and immune cells. J Immunother Cancer 7:305. https://doi.org/10.1186/s40425-019-0770-2
36. Oba T, Long MD, Keler T et al (2020) Overcoming primary and acquired resistance to anti-PD-L1 therapy by induction and activation of tumor-residing cDC1s. Nat Commun 11:5415. https://doi.org/10.1038/s41467-020-19192-z
37. Wen Z, Wang J, Tu B et al (2023) Radiofrequency ablation combined with toripalimab for recurrent hepatocellular carcinoma: a prospective controlled trial. Cancer Med 12:20311–20320. https://doi.org/10.1002/cam4.6602
38. Wang X, Liu G, Chen S et al (2021) Combination therapy with PD-1 blockade and radiofrequency ablation for recurrent hepatocellular carcinoma: a propensity score matching analysis. Int J Hyperthermia: Official J Eur Soc Hyperthermic Oncol North Am Hyperth Group 38:1519–1528. https://doi.org/10.1080/02656736.2021.1991011